Proof, not final version

Article

Journal of
Nanoscience and Nanotechnology
Vol. 15, 1–6, 2015
www.aspbs.com/jnn

Copyright © 2015 American Scientific Publishers
All rights reserved
Printed in the United States of America

Proof, not final page

Solvent-Assisted Preparation of High-Performance Mesoporous $CH_3NH_3PbI_3$ Perovskite Solar Cells

Zhi-Hua Li†, Jie Liu†, Jing-Yuan Ma, Yan Jiang, Qian-Qing Ge, Jie Ding, Jin-Song Hu*, and Li-Jun Wan

Beijing National Laboratory for Molecular Sciences, CAS Key Laboratory of Molecular Nanostructure and Nanotechnology, Institute of Chemistry, Chinese Academy of Sciences (CAS), Beijing 100190, China

Organometal trihalide perovskite based solar cells have attracted great attention worldwide since their power conversion efficiency (PCE) have risen to over 15% within only 3 years of development. Comparing with other types of perovskite solar cells, mesostructured perovskite solar cells based on $CH_3NH_3PbI_3$ as light harvesting material have already demonstrated remarkable advance in performance and reproducibility. Here, we reported a mesoscopic $TiO_2/CH_3NH_3PbI_3$ heterojunction solar cell with uniform perovskite thin film prepared via solvent-assisted solution processing method. The best performing device delivered photocurrent density of 20.11 mA cm^{-2}, open-circuit voltage of 1.02 V, and fill factor of 0.70, leading to a PCE of 14.41%. A small anomalous hysteresis in the *J–V* curves was observed, where the PCE at forward scan was measured to be 84% of the PCE at reverse scan. Based on a statistical analysis, the perovskite solar cells prepared by the reported method exhibited reproducible and high PCE, indicating its promising application in the fabrication of low-cost and high-efficiency perovskite solar cells.

Keywords: Perovskite Solar Cells, Solvent-Assisted, Mesostructured, High-Performance.

1. INTRODUCTION

With increasing industrialization and a growing population, the development of clean alternatives to current power generation system is becoming immensely important. Solar energy is one of the most promising renewable energy sources among all the available forms. At present, crystalline and polycrystalline silicon devices dominate the photovoltaic market; however, the high production and installation costs decrease its viability for widespread use.[1] Organic–inorganic hybrid perovskite solar cells, based on mesoscopic metal oxide or planar heterojunction, have already demonstrated the efficiency exceeding 15% in less than three years, which is becoming the rising star in photovoltaic research.[2–11] The term of hybrid organic–inorganic perovskite is given to a class of compounds that have a general chemical formula AMX_3 (where A is an organic cation, M is a divalent metal ion, and X is a halide or any mixture thereof) such as $CH_3NH_3PbI_3$.[12] $CH_3NH_3PbI_3$, the primary semiconductor of interest, is of high crystallinity and nearly defect free with attractive properties including high optical absorption coefficients and long range balanced electron–hole transport lengths,[13–26] can be manufactured by simple solution processing or scalable vapour phase deposition methods.[5, 6, 27] So far, five main deposition methods have been reported including one-step precursor deposition,[2, 4] sequential deposition process,[5, 28, 29] vapour-assisted two-step reaction process,[30] dual source vacuum deposition and sequential vapour deposition.[6, 31] However, all those approaches suffer from problems such as inadequate surface coverage, insufficient conversation of PbI_2, complicated fabrication procure or excessively energy consumption.[32–35] Recently, Cheng and co-workers reported a planar perovskite solar cell prepared by one-step, solvent-assisted solution method that can obtain high-quality films with densely packed grains of $CH_3NH_3PbI_3$ and thus improved the PCE of the devices.[36]

Here, we report a solvent-assisted solution processing fabrication of high efficiency mesostructured $CH_3NH_3PbI_3$ perovskite solar cells. This simple technique comprises the spin-coating of $CH_3NH_3PbI_3$ precursor onto a mesoporous

*Author to whom correspondence should be addressed.
†These two authors contributed equally to this work.

Proof, not final page

titania scaffold (mp-TiO_2), followed immediately by introducing second solvent to the wet film to regulate the kinetics of nucleation and crystal growth. A highly uniform perovskite active layer was obtained at the top of mp-TiO_2 layer to achieve a lighter absorber layer with bilayer structure which is effective for sufficient light absorption and charge collection. As a result, the perovskite solar cell prepared with solvent-assisted spin-coating technique has achieved a PCE of 14.41% under an illuminating area of 0.16 cm^2. Moreover, comparing with planar structure, the anomalous hysteresis of mesostructured device is relatively small and the device performance is better. Building on these very promising initial results and with further subtle control of carrier dynamics through the entire device, it is expected that a substantial increase in efficiency can be achieved and the anomalous hysteresis can be further ameliorated after further optimization of processing parameters with this technique.

2. EXPERIMENTAL DETAILS

2.1. Solar Cell Fabrication

CH_3NH_3I were first synthesized by the reaction of 24 mL CH_3NH_2 (40% in methanol, Sigma-Aldrich) and 10 mL HI (57 wt% in water, Sigma-Aldrich) in a 100 mL round-bottom flask at 0 °C for 2 h under stirring. The solvents were removed by rotary evaporation at 50 °C for 1 h, and the obtained white solid was washed with anhydrous diethyl ether and finally recrystallized with ethanol. The precursor solution of perovskite was prepared by mixing CH_3NH_3I with PbI_2 (99%, Sigma-Aldrich) at 1:1 mole ratio in anhydrous *N*,*N*-dimethylformamide (99.8%, Sigma-Aldrich) at room temperature for 20 min, and used for *in situ* formation of $CH_3NH_3PbI_3$.

Fluorine-doped tin oxide-coated glass substrate (FTO, Pilkington, TEC8) were patterned by laser cutting and cleaned by ultrasonication with deionized water, ethanol, acetone and isopropyl, respectively. The FTO substrate was then subjected to an UV/Ozone treatment for 20 min. A 60∼70 nm thick TiO_2 blocking layer was deposited on the substrates by spray pyrolysis using a titanium diisopropoxide bis(acetylacetonate) solution (75% in 2-propanol, Sigma-Aldrich) diluted in 1-butanol (1:39, volume ratio) at 450 °C. A 250∼300 nm thick mesoporous TiO_2 layer composed of ∼20 nm nanoparticle was deposited by a two-step spin-coating process at 500 r.p.m. and 4,500 r.p.m. for 5 s and 30 s, respectively, with a commercial TiO_2 paste (Dyesol 18NRT, Dyesol) diluted in ethanol (1:5, weight ratio). After drying at 125 °C for 30 min, the as-deposited TiO_2 films were gradually heated to 525 °C in air, and then baked at this temperature for 30 min to remove organic components. Prior to their use, the films were treated with UV/Ozone treatment for 20 min. Then 60 μL $CH_3NH_3PbI_3$ precursor was coated onto the mp-TiO_2/bl-TiO_2/FTO substrate (around 1.8 cm × 1.8 cm) by spin-coating process at 5,000 r.p.m in the glove box. 180 μL anhydrous chlorobenzene (99.8%, Sigma-Aldrich) was dropped onto the centre of the substrate quickly after the spin-coating process. The obtained film was dried at 100 °C for 10 min. After cooling to room temperature, 60 μL spiro-OMeTAD solution was spin-coated on the perovskite layer as the hole transport layer (HTL). The spiro-OMeTAD solution was prepared by dissolving 72.3 mg spiro-OMeTAD (99.1%, Luminescence Technology Corp.) in 1 mL chlorobenzene. After 20 min stirring at room temperature, 28.8 μL 4-tert-butylpyridine (96%, Sigma-Aldrich), 17.5 μL of a stock solution of 520 mg mL^{-1} lithium bis(trifluor-omethylsulphonyl) imide (99.95%, Sigma-Aldrich) in acetonitrile (99.8%, Sigma-Aldrich) were added and stirred continuously for 3 h. Finally, 80 nm of gold was thermally evaporated on the top of the device as a back contact.

2.2. Characterization

Scanning electron microscopy (SEM) images were recorded on a FEI Helios NanoLab 600i microscopy operating at 5 kV. X-ray diffraction (XRD) data were collected with a Regaku D/Max-2500 diffractometer equipped with a Cu Kα_1 radiation ($\lambda = 1.54056$ Å, Rigaku Corporation, Tokyo, Japan). Current–voltage characteristics were measured with a solar simulator (Newport, USA) equipped with 450 W Xenon lamp (OSRAM) and a Keithley 2420 source meter. The EQE was measured using a power source (IQE 200™, ORIEL). Light intensity was adjusted using a NERL-certified Si solar cell with a KG-2 filter for approximating AM 1.5G light (100 mW cm^{-2}). The active area of solar cells were defined by a 0.16 cm^2 non-reflective metal mask.

3. RESULTS AND DISCUSSION

Figure 1 presents a schematic diagram of the cell architecture and a cross-section SEM image of a typical device. The mesoporous TiO_2 film had an optimized thickness of around 300 nm and was filled with perovskite nanocrystals. A ∼150 nm perovskite photoactive layer lies uniformly at the top of mp-TiO_2 layer. This bilayer-perovskite structure is effective for light harvesting and charge carrier extraction.[26] HTM layer of spiro-OMeTAD is ∼150 nm thick. For this device structure, the morphologies of perovskite capping layer was found to play an extremely important role and influence the PCE dramatically. We found the solvent-assisted methods is an effective technique for creating high quality perovskite capping layer. The solvent-assisted spin-coating procedure is described schematically in Figure 2. Based on traditional one-step spin-coating method, chlorobenzene was introduced while spinning to assist the formation of uniform and dense perovskite capping layer. By delicately controlling the accelerating rate during spin-coating and the dripping timing, uniform and dense perovskite layers can be obtained after baking. Figures 3(a) and (b) shows the SEM image of

Proof, not final page

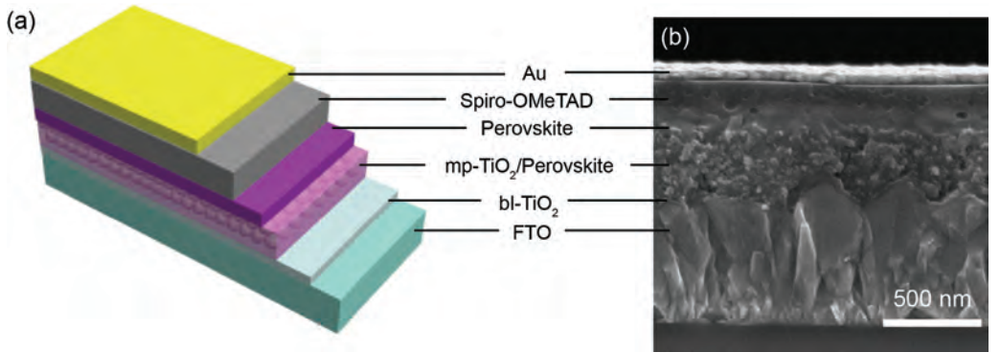

Figure 1. (a) Device structure and (b) cross-sectional SEM image of an optimized perovskite solar cell.

perovskite layers prepared by solvent-assisted spin-coating method. It can be clearly seen that the film made by chlorobenzene-assisted method was much more uniform with lower surface roughness. Atomic Force Microscopy image showed that the root mean square surface roughness (Rq) is 9.94 nm. The crystalline grains in ∼100∼200 nm compactly and fully covered the substrate. In contrast, as shown in Figures 3(c) and (d), the film prepared by conventional method without solvent assistance appears dendritic perovskite structure on the top of mp-TiO_2 layer with relatively poor surface coverage and larger roughness. This dendritic structure will affect the film formation of the HTL and thus deteriorate the device performance.

Furthermore, the crystalline structure of the films were investigated by X-ray diffraction (XRD) technique. Figure 4 presents the typical XRD patterns of the films prepared by solvent-assisted and conventional spin-coating process. Comparing with the control sample without perovskite film, it can be seen that all diffraction peaks except for ones from FTO and TiO_2 in the film prepared by solvent-assisted spin-coating can be well indexed to perovskite $CH_3NH_3PbI_3$.[37] No diffraction peaks from PbI_2 were observed, indicating PbI_2 in the precursor solution was completely converted into perovskite $CH_3NH_3PbI_3$. For the film prepared by the conventional spin-coating process, main diffraction peaks are similar to that of the film prepared by the solvent-assisted spin-coating, except for two weak peaks at 12.42° and 19.78°, which can be attributed to PbI_2. This result indicates that the uniform film with smooth surface and lower roughness are easier to be converted into perovskite.

Both films were then used to fabricate solar cells as described in the experimental section. The J–V curves were measured according to the standard procedure and shown in Figure 5. Solar cells fabricated via the conventional spin-coating method got a PCE of only 8.37%. In contrast, as a result of smooth perovskite capping layer with densely packed grains, the devices utilizing perovskite films prepared by the solvent-assisted method improved significantly in all of the photovoltaic parameters (Table I), leading to a power conversion efficiency (PCE) of 14.41% at standard AM 1.5 G solar illumination. The enhancement of photocurrent density (J_{SC}) is mainly attributed to the continuously capping layer which improved light absorption and reduced defect density that suppressed carrier nonradioactive recombination

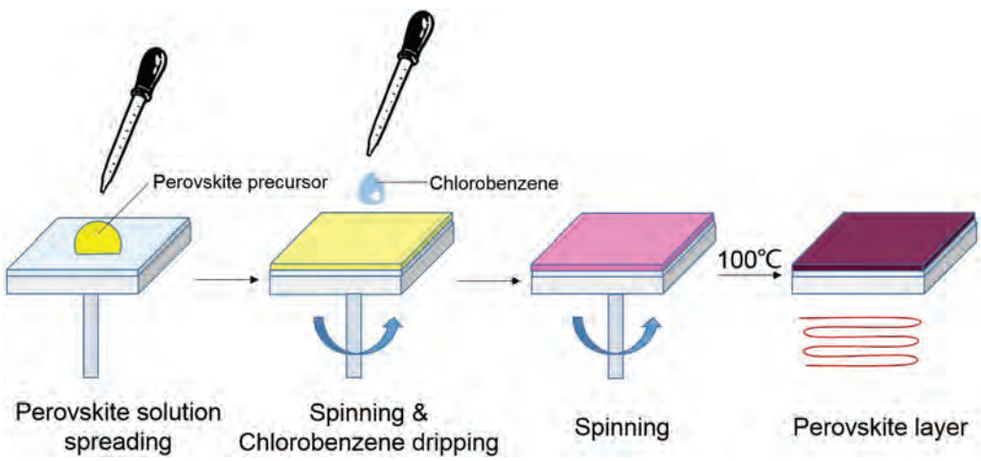

Figure 2. Solvent-assisted spin-coating process for preparing the uniform and dense perovskite film.

Proof, not final page

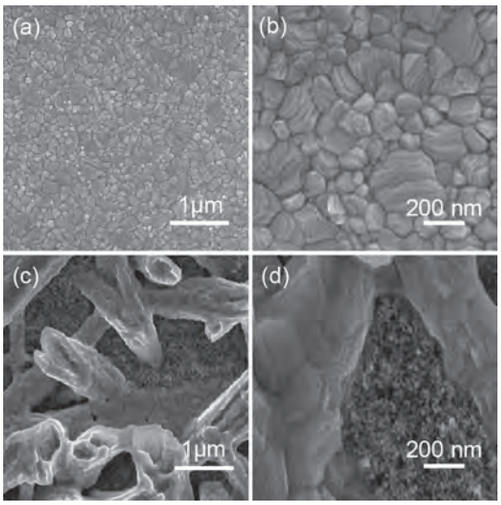

Figure 3. SEM images of $CH_3NH_3PbI_3$ films prepared by solvent-assisted (a), (b) and conventional (c), (d) spin-coating.

channels.[28, 34] It is well recognized that open circuit voltage (V_{OC}) is correlated with the rate of charge extraction and recombination.[38] The improvement of V_{OC} from 0.78 V to 1.02 V clearly indicates a notable increase of charge collection and a decrease of carrier recombination. It has been reported that series resistance (R_s) is the major factor influencing the fill factor (FF) of solar cells. FF will increase as the decrease of R_s. As shown in Table I, comparing to that by conventional method, R_s decreases from 58.66 Ω cm^2 to 29.40 Ω cm^2 for the device prepared by the solvent-assisted method, which results in the increase of FF from 0.64 to 0.70. It is reasonably believed that the improvement of perovskite film quality by solvent-assisted spin-coating contributed to the enhancement of the device performance.

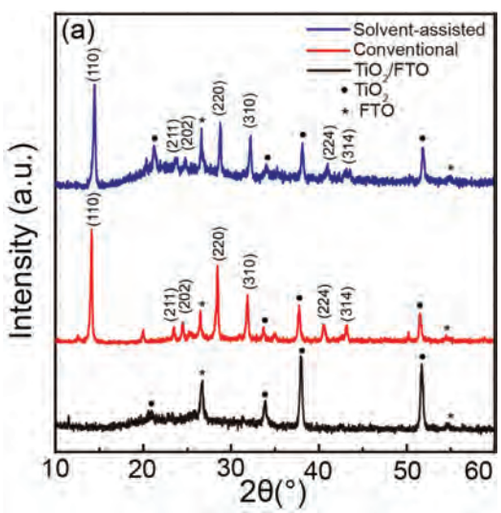

Figure 4. XRD patterns of the $CH_3NH_3PbI_3$ films prepared by solvent-assisted and conventional spin-coating, and the FTO/bl-TiO_2/mp-TiO_2 film for comparison.

It is well known that the perovskite solar cells frequently exhibit J–V anomalous hysteresis depending on voltage scanning direction, so the J–V measurement were tested versus voltage scan direction.[28, 34, 39, 40] Figure 5 presents both J–V curves recorded at the reverse (from V_{OC} to J_{SC}) and forward (from J_{SC} to V_{OC}) scans on the mesostructured $CH_3NH_3PbI_3$ perovskite solar cells prepared by two methods. For the device prepared by solvent-assisted spin-coating, at a scan rate of 13 mV s^{-1}, the J_{SC}, V_{OC} and FF values acquired at the reverse scan were 20.11 mA cm^{-2}, 1.02 V and 0.70, respectively, yielding a PCE of 14.41%. The corresponding values at the forward scan were 19.60 mA cm^{-2}, 0.99 V and 0.63, respectively, leading to a PCE of 12.13% which is about 84% of the PCE at the reverse scan. The average PCE is 13.27%. The external quantum efficiency (EQE) of a typical device shows the onset of photocurrent at 800 nm, consistent with the band gap of $CH_3NH_3PbI_3$ and previous studies.[9] On the other hand, for the device prepared by conventional method, PCE is 8.37% at reverse scan and 5.86% at forward scan, achieving the average PCE of 7.12% (Fig. 5(c)). This value is much lower than that of the device prepared by solvent-assisted spin-coating. Moreover, solvent-assisted method remarkably enhanced the average PCE in a statistical analysis. As shown in Figure 5(b), over 70% devices exhibited a PCE over 13.0% and the average PCE is 13.5% based on statistical analysis on 60 devices prepared by solvent-assisted method. In contrast, the cells prepared by conventional method only demonstrated an average PCE of 6.75% on a basis of 60 devices (Fig. 5(d)). Therefore, these results clearly indicate the morphology and quality of perovskite capping layer in the devices derived from different preparation method significantly affected the device performance.

Furthermore, although the perovskite absorber layers prepared by solvent-assisted method had the similar morphologies in both mesostructured and planar solar cell (Fig. 3), it was found the planar perovskite solar cell showed a lower PCE and larger distortion between reverse and forward scans (Table I). As discussed in previous reports,[39] hysteresis phenomenon may have three possible reasons:

(1) large defect density within or near the surface of the perovskite absorbers;

(2) ferroelectric properties of the perovskite materials, causing a slow polarization occurs when bias voltage is applied;

(3) excess ions as interstitial defects. In the present case, the perovskite film prepared via solvent-assisted technique is of high quality, which effectively reduced the defect density.

By using mesostructured mp-TiO_2 layer in an optimized thickness, charge collection and transport were improved

Proof, not final page

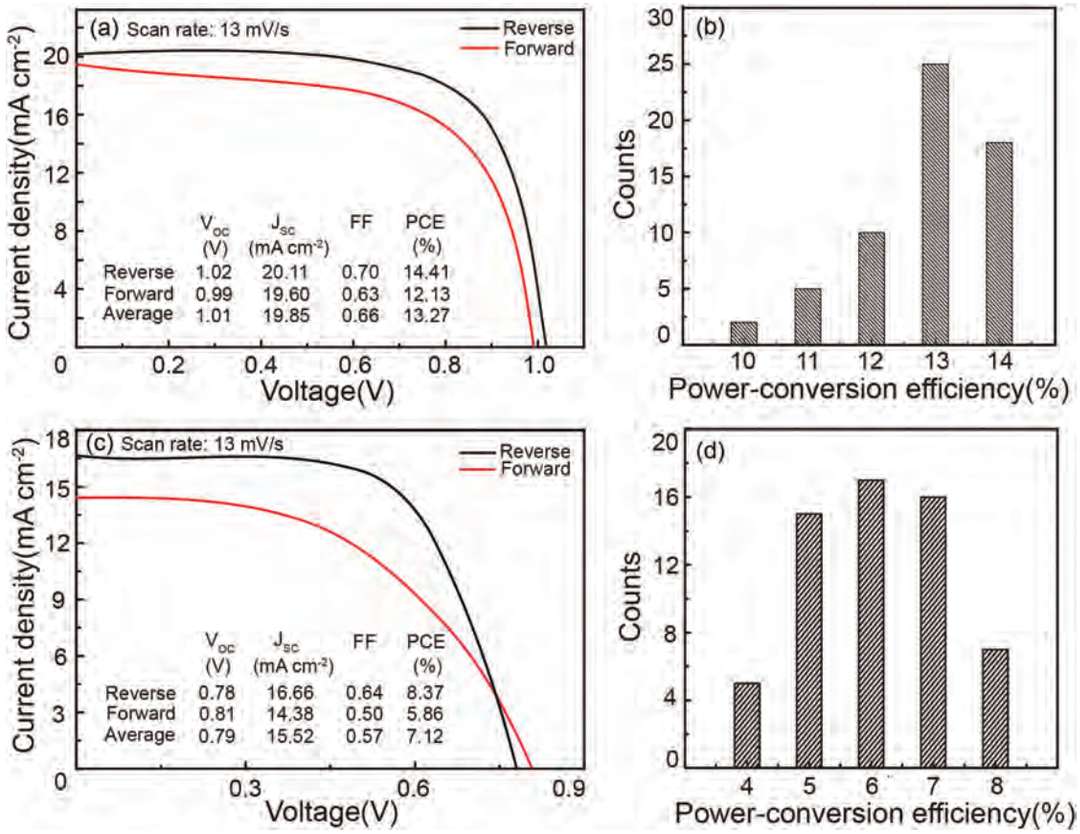

Figure 5. *J–V* curves of the best solar cell recorded at reverse and forward scans, and the statistical analysis of PCE: (a), (b) perovskite solar cells prepared by solvent-assisted spin-coating; (c), (d) perovskite solar cells prepared by conventional spin-coating.

and R_s was effectively reduced in view of the much larger contact of TiO_2 and perovskite, which also facilitated the charge redistribution under reverse or forward biases, and thus relieved the effect of hysteresis. The stoichiometric ratio of perovskite layer was delicately controlled by the precursor solution so that the excess ions can be limited to some extent. We think that all these facts helped to alleviate the hysteresis and distortion in the *J–V* curves.

Table I. Photovoltaic parameters of perovskite solar cells prepared via different methods.

Perovskite solar cells	V_{OC} (V)	J_{SC} (mA cm^{-2})	FF	PCE (%)	R_s (Ω cm^2)
Solvent-assisted method/with 300-nm-thick mp-TiO_2	1.02	20.11	0.70	14.41	29.40
Conventional method/with 300-nm-thick mp-TiO_2	0.78	16.66	0.64	8.37	58.66
Solvent-assisted method/without mp-TiO_2 (planar)	0.98	20.90	0.52	10.66	132.80

4. CONCLUSIONS

In summary, we have successfully applied the solvent-assisted spin-coating technique to prepare mesostructured $CH_3NH_3PbI_3$ perovskite solar cells and achieved a PCE of 14.41%. It was found that this technique is effective to obtain a smooth and compact perovskite capping layer with a low surface roughness on the mesoporous layer, which contributes to the significant improvement of the device performance and the hysteresis between reverse and forward scans. Furthermore, it was also interestingly found that the mesostructured perovskite solar cells prepared by this solvent-assisted method exhibited the increased PCE and reduced hysteresis compared to the planar one fabricated by the same technique. The reported method is compatible with all other organometal trihalide perovskite compounds, and thus should be easily applied to fabricate other perovskite-based solar cells with similar structure for pushing their performance.

Acknowledgments: The authors greatly appreciate the financial support from the National Key Project on Basic Research (2012CB932900, and 2011CB808701), the National Natural Science Foundation of China (91127044 and 21173237), and the Strategic Priority Research

Proof, not final page

Program of the Chinese Academy of Sciences (Grant No. XDB12020100).

References and Notes

1. S. Chu and A. Majumdar, *Nature* 488, 294 (**2012**).
2. M. M. Lee, J. Teuscher, T. Miyasaka, T. N. Murakami, and H. J. Snaith, *Science* 338, 643 (**2012**).
3. A. Mei, X. Li, L. Liu, Z. Ku, T. Liu, Y. Rong, M. Xu, M. Hu, J. Chen, Y. Yang, M. Grätzel, and H. Han, *Science* 345, 295 (**2014**).
4. H. Zhou, Q. Chen, G. Li, S. Luo, T. B. Song, H. S. Duan, Z. Hong, J. You, Y. Liu, and Y. Yang, *Science* 345, 542 (**2014**).
5. J. Burschka, N. Pellet, S. J. Moon, H. B. Robin, P. Gao, M. K. Nazeeruddin, and M. Grätzel, *Nature* 499, 316 (**2013**).
6. M. Liu, M. B. Johnston, and H. J. Snaith, *Nature* 501, 395 (**2013**).
7. A. Kojima, K. Teshima, Y. Shirai, and T. Miyasaka, *J. Am. Chem. Soc.* 131, 6050 (**2009**).
8. J. H. Im, C. R. Lee, J. W. Lee, S. W. Park, and N. G. Park, *Nanoscale* 3, 4088 (**2011**).
9. H. S. Kim, C. R. Lee, J. H. Im, K. B. Lee, T. Moehl, A. Marchioro, S. J. Moon, R. Humphry-Baker, J. H. Yum, J. E. Moser, M. Grätzel, and N. G. Park, *Energy Environ. Sci.* 2, 591 (**2012**).
10. M. Grätzel, *Nat. Mater.* 13, 838 (**2014**).
11. P. Patel and D. Mitzi, *MRS Bulletin* 39, 768 (**2014**).
12. D. B. Mitzi, S. Wang, C. A. Feild, C. A. Chess, and A. M. Guloy, *Science* 267, 1473 (**1995**).
13. G. Xing, N. Mathews, S. Sun, S. S. Lim, Y. M. Lam, M. Grätzel, S. Mhaisalkar, and T. C. Sum, *Science* 342, 344 (**2013**).
14. S. D. Stranks, G. E. Eperon, G. Grancini, C. Menelaou, M. J. Alcocer, T. Leijtens, L. M. Herz, A. Petrozza, and H. J. Snaith, *Science* 342, 341 (**2013**).
15. A. Marchioro, J. Teuscher, D. Friedrich, M. Kunst, R. van de Krol, T. Moehl, M. Grätzel, and J.-E. Moser, *Nat. Photonics* 8, 250 (**2014**).
16. W. J. Yin, T. Shi, and Y. Yan, *Adv. Mater.* 26, 4653 (**2014**).
17. Y. Zhao, A. M. Nardes, and K. Zhu, *J. Phys. Chem. Lett.* 5,490 (**2014**).
18. J. Feng and B. Xiao, *J. Phys. Chem. Lett.* 5, 1278 (**2014**).
19. B. Cai, Y. Xing, Z. Yang, W.-H. Zhang, and J. Qiu, *Energy Environ. Sci.* 6, 1480 (**2013**).
20. J. H. Heo, S. H. Im, J. H. Noh, T. N. Mandal, C.-S. Lim, J. A. Chang, Y. H. Lee, H.-J. Kim, A. Sarkar, M. K. Nazeeruddin, M. Grätzel, and S. I. Seok, *Nat. Photonics* 7, 486 (**2013**).
21. H. S. Kim, J. W. Lee, N. Yantara, P. P. Boix, S. A. Kulkarni, S. Mhaisalkar, M. Gratzel, and N. G. Park, *Nano Lett.* 13, 2412 (**2013**).
22. D. Zhong, B. Cai, X. Wang, Z. Yang, Y. Xing, S. Miao, W.-H. Zhang, and C. Li, *Nano Energy* 11, 409 (**2015**).
23. M. Jin, S. S. Kim, M. Yoon, Z. Li, Y. Y. Lee, and J. M. Kim, *J. Nanosci. Nanotechnol.* 12, 815 (**2012**).
24. H. H. Ko, S. Yi, and S. H. Jeong, *J. Nanosci. Nanotechnol.* 13, 7906 (**2013**).
25. R. Passalacqua, C. Ampelli, S. Perathoner, and G. Centi, *Nanosci. Nanotech. Let.* 4, 142 (**2012**).
26. A. Mathew, G. M. Rao, and N. Munichandraiah, *Sci. Adv. Mater.* 5, 583 (**2013**).
27. D. Liu and T. L. Kelly, *Nat. Photonics* 8, 133 (**2013**).
28. J. H. Im, I. H. Jang, N. Pellet, M. Grätzel, and N. G. Park, *Nat. Nanotechnol.* 9, 927 (**2014**).
29. P. Docampo, F. C. Hanusch, S. D. Stranks, M. Doblinger, J. M. Feckl, M. Ehrensperger, N. K. Minar, M. B. Johnston, H. J. Snaith, and T. Bein, *Adv. Energy Mater.* 4, 1400355 (**2014**).
30. Q. Chen, H. Zhou, Z. Hong, S. Luo, H. S. Duan, H. H. Wang, Y. Liu, G. Li, and Y. Yang, *J. Am. Chem. Soc.* 136, 622 (**2014**).
31. Y. Chen, T. Chen, and L. Dai, *Adv. Mater.* 27, 1053 (**2015**).
32. S. Shi, Y. Li, X. Li, and H. Wang, *Mater. Horiz.* (**2015**), DOI: 10.1039/c4mh00236a.
33. P. Gao, M. Grätzel, and M. K. Nazeeruddin, *Energy Environ. Sci.* 7, 2448 (**2014**).
34. N. J. Jeon, J. H. Noh, Y. C. Kim, W. S. Yang, S. Ryu, and S. I. Seok, *Nat. Mater.* 13, 897 (**2014**).
35. T. Leijtens, B. Lauber, G. E. Eperon, S. D. Stranks, and H. J. Snaith, *J. Phys. Chem. Lett.* 5, 1096 (**2014**).
36. M. Xiao, F. Huang, W. Huang, Y. Dkhissi, Y. Zhu, J. Etheridge, A. Gray-Weale, U. Bach, Y. B. Cheng, and L. Spiccia, *Angew. Chem. Int. Ed.* 53, 9898 (**2014**).
37. J. H. Im, J. Luo, M. Franckevicius, N. Pellet, P. Gao, T. Moehl, S. M. Zakeeruddin, M. K. Nazeeruddin, M. Grätzel, and N. G. Park, *Nano Lett.* 15, 2120 (**2015**).
38. U. Rau, *Phys. Rev. B* 76, 085303 (**2007**).
39. H. J. Snaith, A. Abate, J. M. Ball, G. E. Eperon, T. Leijtens, N. K. Noel, S. D. Stranks, J. T.-W. Wang, K. Wojciechowski, and W. Zhang, *J. Phys. Chem. Lett.* 5, 1511 (**2014**).
40. H.-S. Kim and N.-G. Park, *J. Phys. Chem. Lett.* 5, 2927 (**2014**).

Received: 15 April 2015. Accepted: 23 April 2015.

Proof, not final page